Ultrastructural Organization of Eumelanin from *Sepia officinalis* Measured by Atomic Force Microscopy†

Christine M. R. Clancy‡ and John D. Simon*,‡,§

Department of Chemistry, Duke University, Durham, North Carolina 27708, and Departments of Biochemistry and Ophthalmology, Duke University Medical Center, Durham, North Carolina 27710

Received April 18, 2001; Revised Manuscript Received August 24, 2001

ABSTRACT: Atomic force microscopy is used to investigate the structural organization of eumelanin isolated from the inks sacs of the cuttlefish *Sepia officinalis*. Deposits of eumelanin on mica reveal a range of structures. The most prevalent structure is an aggregate comprised of particles with diameters of 100−200 nm. This morphology is consistent with published SEM images of intact granules. Mechanical manipulation of these structures using the AFM tip show that these particles, while stable, are not a fundamental structural unit but are an aggregate of smaller constituents. Images of the bulk pigments also reveal the presence of filament structures that have an average height and width of ∼5 nm and tens of nanometers, respectively. Taken along with recent X-ray scattering and mass spectrometry experiments, the AFM data provides strong supporting evidence for the conclusion that eumelanin is comprised of small oligomeric units and that the structural morphology observed in imaging experiments reflects aggregation of these oligomeric molecules. On the basis of the types of structures observed in the AFM images, a model is proposed for the assembly of the macroscopic pigment. The diversity of functions attributed to melanin in the literature is proposed to result from the heterogeneity of aggregated structures.

Melanin is an important class of pigments that have attracted attention from a wide range of scientists (*1*−*3*). Melanin is present in different regions within the human body: skin, hair, eye, inner ear, and brain. The proposed functions of melanin are quite diverse, including photoprotection, photosensitization, metal ion chelation, antibiotic, thermoregulation, and free radical quenching (*1*, *4*, *5*). Not all of its effects are positive in regard to human health; there are data that demonstrate that melanin induces DNA damage through its own photoreactions following ultraviolet excitation (*6*−*8*). In principle, the function(s) of the pigment should be related to its structure; however, despite significant experimental effort spent studying a variety of natural and synthetic melanin, the molecular structure and aggregation behavior of melanin is not understood.

There are two distinct types of melanin found in humans: black to brown eumelanin and yellow to red pheomelanin (*9*−*13*). In the present study, we examine eumelanin. Eumelanin is the more ubiquitous melanin pigment and is a biopolymer produced enzymatically from tyrosine via formation of 5,6-dihydroxyindole (DHI) and 5,6-dihydroxyindole-2-carboxylic acid (DHICA) (*14*, *15*). Figure 1 shows the current understanding of the initial steps of eumelanin melanogenesis (*16*). It is possible to make synthetically pure DHI and DHICA melanin. Natural eumelanin, however, are comprised of a DHI/DHICA copolymer and there can be great variability in the relative amounts of these two precursors in the macroscopic pigment (*17*−*21*). At present, the molecular structure of DHI and DHICA eumelanin or the DHI/DHICA copolymer are largely unknown.

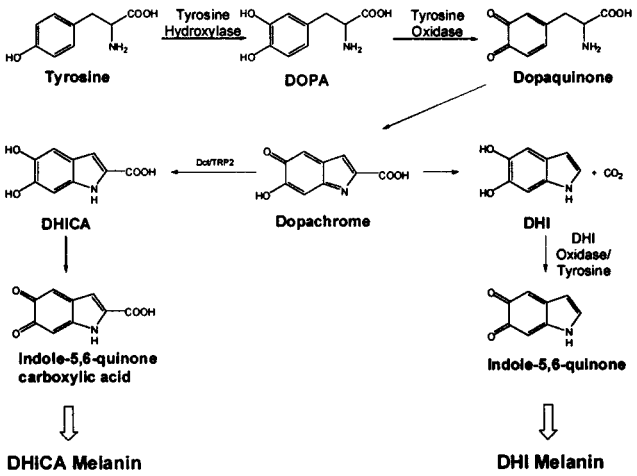

FIGURE 1: Biochemical synthesis pathways of DHI and DHICA eumelanin. Synthetic eumelanins can be generated from the pure precursors DHI and DHICA. Natural eumelanins contain a mixture of these two molecules.

Herein, we examine a natural eumelanin commonly used as a model for the human pigment: eumelanin isolated from the ink sacs of the cuttlefish *Sepia officinalis.* This material can be isolated in quantities large enough to study using physical techniques (*22*). Matrix-assisted laser desorption ionization time-of-flight mass spectrometry (MALDI-TOF MS) studies reveal molecular constituents in *Sepia* as well as other natural and synthetic eumelanin that have molecular

† Supported by National Institute of General Medical Sciences Grant GM-56882.

* To whom correspondence should be addressed. Phone: (919) 660-1508. Fax: (919) 660-1605. E-mail: jds@chem.duke.edu.

‡ Department of Chemistry.

§ Department of Biochemistry.

10.1021/bi010786t CCC: $20.00
Published on Web 10/13/2001

weights between 500 and 1500 amu (*23*−*28*). X-ray diffraction measurements of dried eumelanin have led to the proposal that eumelanin is highly cross-linked planar oligomeric structure that contains ∼4−5 indolequinone-like monomers (*29*, *30*). The pigment is believed to be an aggregate of these π-stacked, cross-linked, planar structures. Support for this model comes from images recorded using scanning tunneling microscopy (STM) (*31*−*33*), small-angle neutron scattering, and small-angle X-ray scattering data on solutions of pure synthetic eumelanin and synthetic eumelanin in the presence of copper ions (*34*).

On a larger distance scale, scanning electron microscopy (SEM) images of *Sepia* eumelanin suggest that the pigment is an aggregated structure comprised of subunits that have a lateral dimension on the order of 150 nm (*35*, *36*). In a recent letter, we compared atomic force microscopy (AFM)[1] and SEM images of *Sepia* eumelanin and showed that AFM can reveal structural features that are not observable using SEM (*37*). In agreement with SEM results, large aggregated structures comprised of ∼150 nm diameter particles are observed. However, a range of smaller particles ∼5−25 nm in diameter appear in the AFM image, suggesting that smaller cohesive entities exist. We also found that the ∼150 nm particles remained intact under mechanical stress.

AFM is a high-resolution imaging technique that can provide three-dimensional topographical information. AFM has been used to image a wide variety of biological materials and molecules, including of single protein molecules, collagen molecules, and amyloid fibers. In this study, we present a detailed AFM study of *Sepia* eumelanin. Our data demonstrate a range of structures: filaments, isolated particles (∼5 to ∼200 nm in dimension), and aggregates of particles. Through manipulation of these entities, we are able to demonstrate that these constituents are not independent, but are built from a common origin. Using these results, a model for the assembly of the eumelanin pigment is proposed. It is reasonable to hypothesize that the range of chemical and photochemical behavior exhibited by this pigment is linked to aspects of its structure.

EXPERIMENTAL PROCEDURES

Materials. Eumelanin from the ink sacs of *Sepia officinalis* was obtained from Sigma Chemical Company (St. Louis, MO) and used without further purification. Deuterated water (D_2O) was purchased from Cambridge Isotopes. HPLC-grade water was purchased from Mallinckrodt Chemical.

Preparation of Eumelanin Samples. Eumelanin was added to either deuterated water or HPLC-grade water at the ratio of 1 g of eumelanin to 1 L of solvent. The solution was then sonicated (Branson Ultrasonics Corporation) for 30 min at a temperature between 18 and 23 °C and then centrifuged (RC-5 Superspeed Refrigerated Centrifuge, DuPont Co., Sorvall Centrifuge Products) at 3000 rpm for 30 min. We will refer to the decanted eumelanin solution following centrifugation as the stock solution. An Amicon stirred cell equipped with ultrafiltration disk membranes (Amicon, Millipore) was used to separate the stock solution into different molecular weight (MW) fractions. The ultrafiltration disk membranes are rated in terms of MW by their ability to retain globular proteins. By use of a series of membranes, solutions could be prepared that represented the following mass ranges: MW > 10 000, 10 000 > MW > 3000, 3000 > MW > 1000, MW < 1000. In terms of molecular size, the MW 10 000 cutoff membrane retains >95% and the MW 3000 cutoff retains >98% of cytochrome C, respectively. From crystallographic and AFM studies, the diameter of cytochrome C is on the order of 3 nm (*38*). All filtration was performed at 5 °C.

Atomic Force Microscopy. AFM images (height, amplitude, and phase) were collected using a Digital Instruments Nanoscope IIIa Bioscope AFM operated in tapping mode (TM). Height and deflection measurements were collected with the same apparatus operated in contact mode (CM). The AFM head was mounted on a Zeiss Axiovert 100TV inverted optical microscope allowing visual observation of the sample. TM imaging was performed using 125 mm long silicon diving board cantilevers with spring constants of ∼30 N/m, tips of nominal radii of ∼5−10 nm and tip half-angles of 10° (back) and 25° (front) (Digital Instruments, Santa Barbara, CA). The frequency of cantilever oscillation was 280−320 kHz. CM imaging was performed using 100 and 200 μm long silicon nitride cantilevers with spring constants of ∼0.6 and 0.1 N/m and tips with nominal radii of ∼20−60 nm. Images were collected at 512 × 512 pixel resolution. Scan rates were between 0.3 and 2 Hz (tip velocities on the order of 10 μm/s) in TM and 2−15 Hz (∼10−150 μm/s) in CM. In TM, phase imaging was performed in the hard and soft tapping limits, and no qualitative differences were found in the phase shifts of the features in the collected images. Images were either left unprocessed or were plane-fit (first order) and/or flattened (zeroth order) with DI Nanoscope software so that the features in the images could be more clearly seen and quantitative measurements more accurately made. Widths and heights of eumelanin structures were found by analyzing cross-sections using DI Nanoscope software. All features discussed were observed in both D_2O and H_2O eumelanin solutions.

Eumelanin was cut using the tip of a silicon AFM tapping mode probe. After collecting an image of the sample, a cut was made by a three-step process. First, the slow scan feature was disabled, leaving the AFM probe to repeatedly pass over the same axis of the sample. Second, the AFM tip was driven into the eumelanin sample by lowering the feedback setpoint; this procedure forces the cantilever oscillation to be dampened by increasing the force of interaction between the tip and the sample. Finally, the scan rate was increased such that tip velocities on the order of tens of micrometers per second were achieved. Profile changes were observed in the scope trace as cutting was performed. Generally, cutting would last tens of seconds. Imaging would then be resumed under normal parameters.

The surface of deposited materials was removed by using normal imaging conditions except that the scan rate was raised to 5.09 Hz (a tip speed of 81.4 μm/s) for 45 min. (Normal scan rates are ∼1 Hz and ∼10 μm/s.) AFM samples were prepared by deposition of several drops of eumelanin

[1] Abbreviations: AFM, atomic force microscopy; TM, tapping mode; CM, contact mode; MW, molecular weight; DHI, 5,6-dihydroxyindole; DHICA, 5,6-dihydroxyindole-2-carboxylic acid; MALDI-TOF MS, matrix-assisted laser desorption ionization time-of-flight mass spectrometry; SEM, scanning electron microscopy; STM, scanning tunneling microscopy.

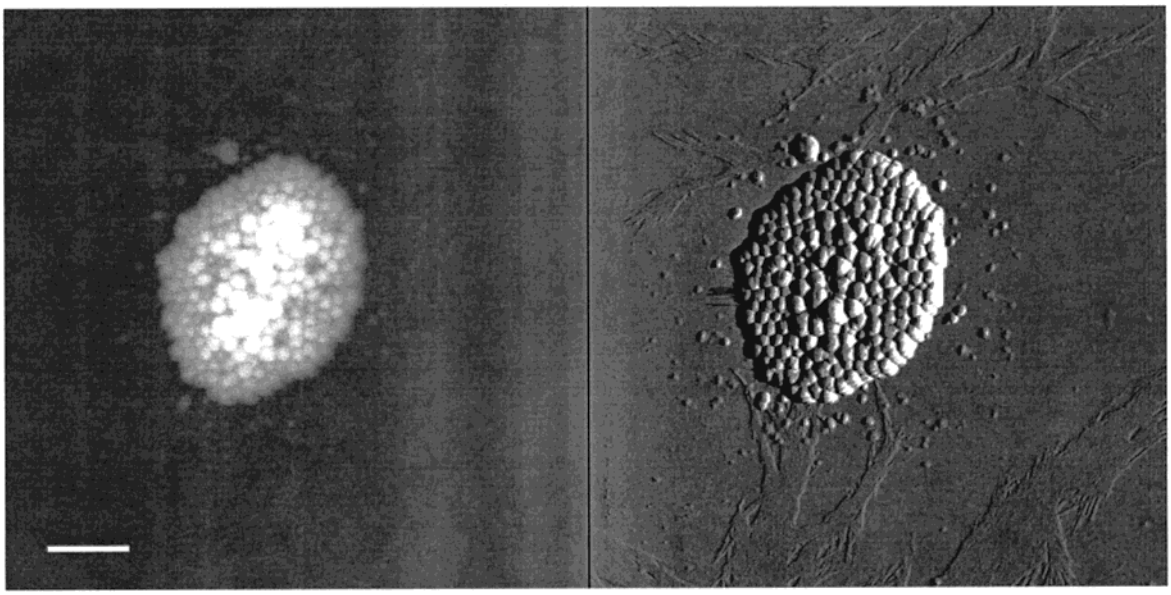

FIGURE 2: Contact mode AFM height (left) and deflection (right) images of a typical *Sepia* eumelanin aggregate deposited on mica from stock eumelanin solution. Smaller eumelanin particles are observed surrounding the micron-sized aggregate, and filaments are seen on much of the surface; this is most easily in the deflection image. The scale bar is 970 nm.

solution onto a freshly cleaved mica surface. The samples were allowed to dry in the dark.

RESULTS

TM and CM AFM images were collected of dried *Sepia officinalis* stock eumelanin on freshly cleaved mica. In general, TM images were of higher quality and better spatial resolution than CM images. When the sample was viewed through the optical microscope with either a 10× or 40× objective, the most noticeable features were large, black to brown, round, and doughnut-shaped deposits. These deposits are too large to image because they are taller than the tolerance of the AMF in the vertical *z* direction (∼6 μm). When the tip did encounter one of these deposits, the material would generally stick to the cantilever and render the tip unusable. These features, however, had the same general appearance as those characterized by previous SEM studies (*36*, *39*, *40*). In the discussion that follows, height, amplitude, and phase data are discussed. Height data provides three-dimensional, topographical information of the sample. The amplitude image is sensitive to changes in the slope as a function of spatial coordinate and, therefore, is useful for identifying edges. Phase data measures the phase shift in the cantilever oscillation from that of the driving force, which results from attractive and repulsive interactions between the AFM tip and the sample. Thus, this signal can be related to the stiffness of the sample and is useful for revealing domains that may otherwise be hidden, overlooked, or difficult to see in the height and amplitude images. In contact mode, height data also provides topographical information, and deflection data is equivalent to the amplitude data in tapping mode.

Another feature frequently and consistently observed through the optical microscope was smaller structures that the AFM revealed to be ∼1 μm in size (see Figure 2). These structures have significant substructure, as seen in the height and deflection images in Figure 2. These images reveal that micron-sized eumelanin deposits are aggregated structures comprised of entities that appear to have diameters on the order of one to two hundred nanometers. This structural morphology is characteristic of *Sepia* eumelanin and is consistent with previous SEM and AFM studies. The structural morphology of the aggregate is not affected by repeated scanning. The images in Figure 2 also reveal the presence of individual particles surrounding the large aggregated structure and there are also regions of the surface that appear to be coated with a smooth material.

The deflection image shown in Figure 2 clearly reveals three distinct types of eumelanin structures. First, small particles with lateral dimensions of ≥20 nm and heights of 4−15 nm heights are observed. Second, isolated particles ∼150 nm in diameter are observed. Third, filament structures are observed surrounding the aggregate. The shape of the isolated particles is also not affected by repeated scanning. The effect of repeated scanning of the filament structures is addressed below.

In an experiment to determine whether the ∼150 nm particles are fundamental polymeric units, Figure 3a shows the results of using the tip of the AFM to cut across one of the ∼1 μm structures. The left side of Figure 3a shows the aggregate as imaged in TM. The right side of Figure 3a shows the image obtained after using the AFM TM tip to scribe a line across the material. The width and depth of the cut is consistent with the dimensions of the AFM tip. A ridge has been generated on the two sides of the cut. Figure 4b shows the height profiles along the solid white lines in the images shown in Figure 4a. The cut is ∼30 nm deep and ∼30 nm wide. The ridge regions immediately adjacent to the cut are ∼20 nm higher than in the initial image.

To focus attention on the smaller building blocks of the pigment, images were collected on a dried 1000 < MW < 3000 eumelanin sample. For this sample, significant regions of the mica are covered with a filament structure, as exemplified by the ease of finding these structures all across the mica surface. Representative height and phase images of these filaments are shown in Figure 4a. Figure 4b is a cross section of the height of the material along the solid

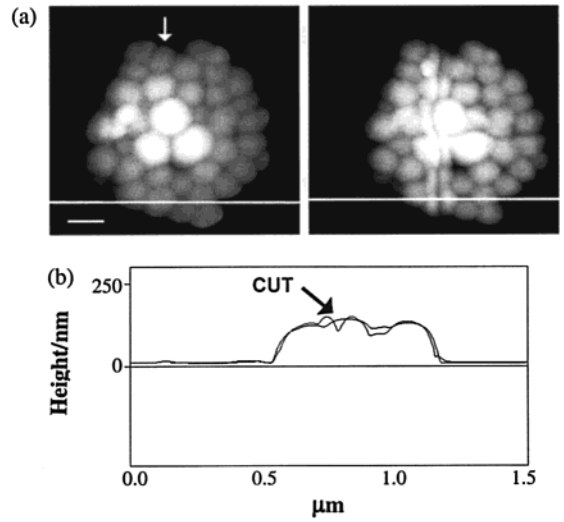

FIGURE 3: (a) Tapping Mode AFM height images of a large eumelanin aggregate dried on mica from stock eumelanin solution before (left) and after (right) the AFM tip was used to cut into the aggregate along the white arrow. The scale bar is 210 nm. (b) Cross sections of the aggregate before and after cutting taken along the white lines in panel a. The cut is ~30 nm deep and there is a build-up of material on the edge of the cut. There is also a change in the region ~300 nm to the right of the cut that arises because the particle on the edge of the aggregate adjacent to the one that is cut is slightly displaced by the cutting of the aggregate.

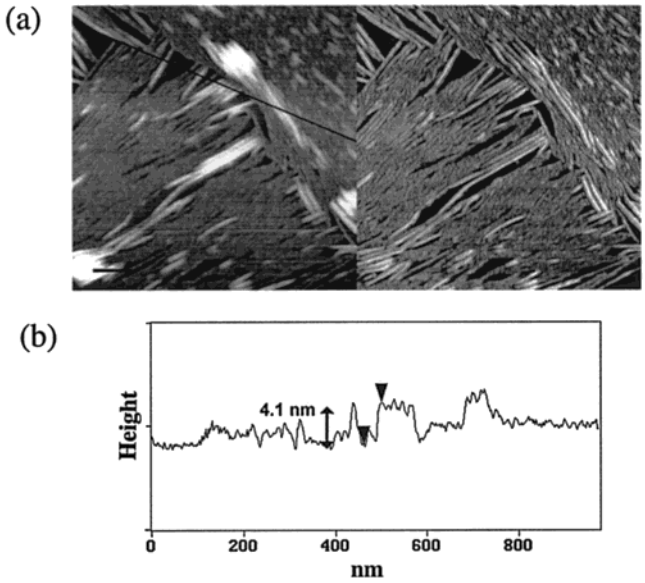

FIGURE 4: (a) Tapping Mode AFM height (left) and phase (right) images of eumelanin filaments dried on mica from the 1000 < MW < 3000 *Sepia* eumelanin fraction. The scale bar is 125 nm. (b) Cross section of the filaments in panel a taken at along the black line in the height image. These data show that the filaments are ~3−6 nm in height and approximately 15−50 nm in diameter.

black line drawn in the height image in Figure 4a. These data show that the filaments are between 3 and 6 nm in height, ~15−50 nm in diameter (this is probably larger than the actual dimension and is convoluted by the AFM tip), and often several microns in length. Figure 5 examines a region of the filaments in Figure 4 containing a large number of these structures that is scanned repeatedly. Figure 5a is the initial scan of the region; Figure 5b shows the same region after repeatedly scanning and acquiring images of the same area for 52 min under normal scanning conditions and

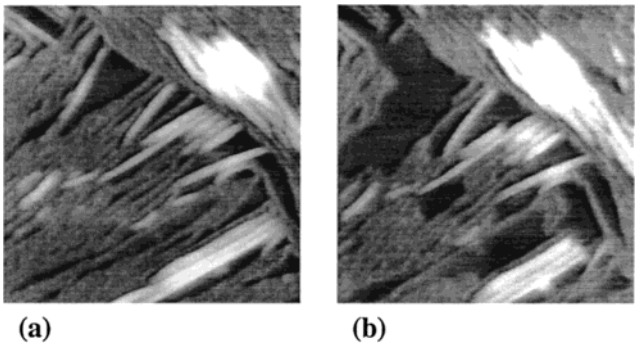

FIGURE 5: Tapping Mode AFM height images of the same area of filaments in the 1000 < MW < 3000 *Sepia* eumelanin fraction sample (a) before and (b) after repeated image collection under normal scanning conditions. Filaments have been destroyed and material apparently removed from the area in the image. The images are 460 nm square.

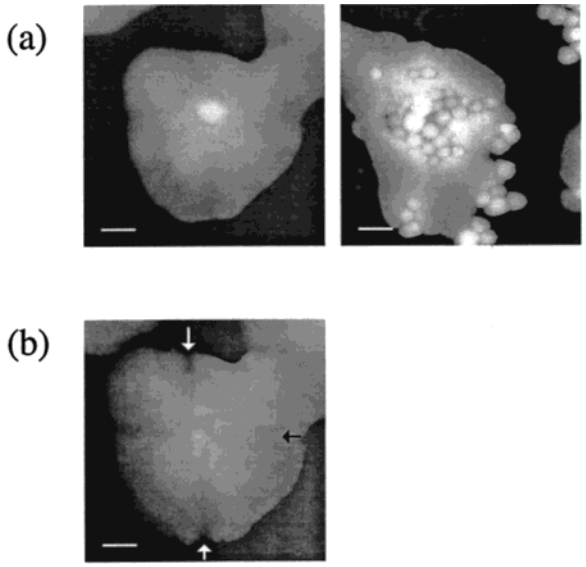

FIGURE 6: (a) Tapping Mode AFM height images of amorphous aggregates found in stock eumelanin dried on mica. The scale bar is 237 nm. The scale bar in the image on the right is 350 nm. (b) Tapping Mode AFM height image of the same aggregate on the left in panel a after cutting with the AFM tip vertically (white arrows) and then horizontally (black arrow) followed by fast rastering of the AFM tip across the scan area for 45 min. The scale bar is 237 nm.

a tip velocity of 4.88 μm. The act of scanning appears to remove the filaments from the surface, as no debris material was imaged in a larger scan area after the damage was observed.

Finally, structures are observed that appear to have no discernible substructure; Figure 6a shows two examples of such deposits. The image on the left exhibits a single ~150 nm particle in the middle of a deposit that exhibits no substructure. The image of the right shows a deposit that has intermittent areas similar to Figure 2 separated by amorphous material. The particular deposit shown in the left image in Figure 6a was cut along the indicated arrows as described above and then the AFM tip was used to displace the top layer of material as described in the Experimental Procedures. This resulted in the image shown in Figure 6b, which shows structures similar to that observed in Figure 2. The center particle in Figure 6a is not present in the latter image because of the manipulation of the material by the AFM tip.

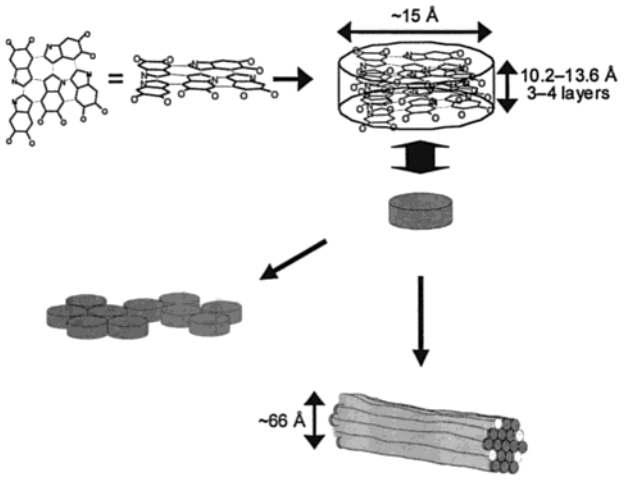

FIGURE 7: A schematic diagram of the initial assembly of eumelanin based on results from previously published scattering and imaging studies. The fundamental molecular unit is taken to be a small planar oligomer built from ~5 DHI/DHICA units. This planar oligomer assembles through π-stacking and side-on interactions. The assembly is consistent with the filaments shown in Figures 4 and 5, and it is likely that the large particles are formed starting in this manner. Spectroscopic studies show a range of oxidation states present in eumelanin (quinone, semiquinone, hydroquinone). This diversity in oxidation states is likely important in enabling the side-on association between the planar oligomers as it will enable hydrogen bonding interactions between the edges of the oligomers.

DISCUSSION

AFM images of eumelanin isolated from *Sepia officinalis* reveal three different structural motifs: filaments, individual particles ranging in size from less than 10 nm to several hundred nanometers, and aggregated structures comprised of individual particles. The information contained in these images provides insight into the structural organization of eumelanin. Before discussing the structural organization of eumelanin, there are two points which need to be discussed. First, it is important to point out that the substrate used, mica, is weakly negatively charged. In principle, a charged surface could influence the assembly of the pigment and generate structures driven by electrostic interactions not present in the native material. As we discuss below, the structural organization revealed by the AFM images is consistent with previous SEM studies, which are not performed on charged substrate. Thus, the mica does not influence the structural feature of eumelanin, and AFM can be used to probe structural details that are not easily discerned using techniques such as SEM. Second, eumelanin is a soft material and one needs to determine if scanning alters its structure. All features, except filaments (discussed in detail below), are unaffected by repeated scanning. Thus, the structural organization observed is not altered by the act of scanning.

We now focus on the highest aspect ratio structure observed, the filaments (Figures 4 and 5). Filaments are found in the AFM images of dried stock and mass-restricted fractions of *Sepia* eumelanin solutions. Some of the highest quality images of isolated filaments were obtained for the $1000 < MW < 3000$ fraction. Heights and widths of 16 filaments that are not adjacent to or bundled with other filaments were measured from TM AFM data. The average filament height and diameter are 4.8 and 35 nm, respectively.

This type of fibrous structure is not unprecedented in biological systems. There are many examples in the literature of biological materials that can organize into fibers and filaments, e.g., synthetic peptides and amyloid polypeptides (*41*−*45*). While the basic molecular building block of eumelanin remains unknown, relevant information concerning its structure is available from X-ray scattering, scanning probe microscopy, and MALDI-TOF MS studies. From a fit to X-ray scattering data of *Sepia* eumelanin and two synthetic eumelanins, the fundamental molecular unit of eumelanin was proposed to be a small planar oligomer consisting of ~5 indole units, see Figure 7 (*29*). This oligomer is consistent with the mass range observed for MALDI-TOF MS data on various types of eumelanin. However, the highly cross-linked structure is different than the linear oligomers proposed from mass spectral data (*23*−*28*). Further, the best fit of the scattering data was obtained using a model of three to four such structures π-stacked together. This structure is labeled the "fundamental aggregate" and is shown in Figure 7 as a stack of three eumelanin oligomers measuring ~15 Å across and 10.2−13.6 Å deep. The fundamental aggregate is also represented in Figure 7 as a gray cylinder. Evidence in support of a stacked structure was recently reported in a STM and TM AFM study of unbleached and mildly bleached synthetic eumelanin (*31*, *32*). The data described supported the existence of eumelanin aggregates that have the same overall dimensions as the proposed π-stacked fundamental aggregate structure. The heights of the observed eumelanin structures were smaller for bleached eumelanin samples than for unbleached samples. This implies a disruption in π-stacking aggregation by bleaching which results in the imaging of single oligomers in the bleached samples versus imaging of fundamental aggregates in the unbleached samples. The widths of melanin particles imaged in the STM work also support the cross-linked Cheng oligomer and not a linear oligomer (*32*).

Evidence in support of this general model also comes from recent small-angle X-ray scattering experiments on synthetic eumelanin alone and in the presence of copper ions (*34*). In the absence of metal and at low Cu ion concentrations, structural components consisting of sheets of thickness of ~12−13 Å are proposed. This thickness is consistent with the fundamental aggregate height, and the authors proposed edge-to-edge aggregation of fundamental aggregates as shown in Figure 7, bottom left. At intermediate Cu ion concentrations, rodlike aggregates with radii of 32.8 Å were formed. These rods were attributed to aggregates of π-stacked melanin oligomers. The structure of these rods is depicted in Figure 7, bottom right. Except for the planar oligomer (*29*), these various structures observed should be held together by noncovalent interactions. The two images presented in Figure 5 shows how the topology of sample changes upon repeated TM imaging. The act of scanning clearly disrupts the integrity of the material; this is best evidenced by the creation of a region near the center of the image that was previously occupied by fibers. In addition, along the edge of this region, we observe short structures that are remnants of some of the long fibers observed prior to repeated imaging. The central importance of π-stacking in the assembly of eumelanin is confirmed by the fact that the morphology of the filaments can be changed under normal scanning conditions. However, these data argue that there is stability in the formation of a π-stack between such

molecular units, and it is reasonable to conclude that such interactions can play an important role in the assembly of the macroscopic pigment

We now turn our attention to the particles revealed in Figure 2. The particles observed range in size from less than tens to hundreds of nanometers. For discussion purposes, we will divide the observed melanin particles into two general classes: <100 nm, and >100 nm, realizing that the latter are the building blocks of the large aggregates such as those in Figure 2. Previous SEM studies were interpreted as suggesting that the >100 nm particles comprising eumelanin aggregates are essentially spherical (*36*, *39*). Herein, we address this particular question as well as the issue of whether these particles are fundamental molecular entities or aggregates of smaller building blocks, as we concluded for the filaments above.

The heights of the <100 nm particles in TM AFM images are measured to be between 4 and 15 nm. Lateral dimensions of these particles range from 40 to 80 nm. These sizes were determined by taking a cross-section of each particle and measuring from the base on one side to the base on the other. There is no observed correlation between height and width; particles with heights between 4 and 5 nm have a range of widths similar to particles with heights falling in the 5−6, 6−7, 7−8, 8−9, and greater than 9 nm.

The large particles, which measure ∼150 nm in height and ∼200 nm in width, are generally found associated in large aggregated structures rather than isolated as single particles on the mica surface. Previously, we reported that when an AFM tip is repeatedly lowered into and raised out of one point in the sample, eumelanin adheres to the AFM tip (*37*). For a eumelanin deposit that is 100−200 nm deep, material extends approximately 1.5 μm up the tip, or 2.2 μm along the angled side of the tip, implying that the pigment pushes itself up the tip upon multiple exposures into the sample. In general, the material that is picked up does not coalesce into a single particle. Instead, the material shows a variety of shapes. Several ∼150 nm particles were picked up by the tip and remained intact. The ability of the AFM tip to pick up the ∼150 nm spherical particles indicates that these are stable structures, a conclusion supported by the observation of an occasional isolated particles on the mica surface (Figure 2).

Despite the stability these large particles display, AFM images suggest that they may be aggregates of smaller structures. In an effort to address this issue directly, the AFM tip was used to cut across a collection of the particles. The before and after images associated with this experiment are shown in Figure 3. The AFM tip creates a clean cut across the material. The depth and width of the cut are ∼30 nm, only a fraction of the height of the material on the surface. The region adjacent to the cut is ∼20 nm higher than in the initial image. This suggests that material is displaced from the center of the cut to the edge of the cut as the AFM tip was moved through the material. These observations indicate that the size of the eumelanin unit displaced by this perturbation is small compared to the dimensions of the AFM tip. These results enable us to definitely conclude that the ∼150 nm eumelanin particles are not a fundamental structural units, but are instead themselves aggregated structures. These larger particle must then be composed of small molecular units, just like the filaments.

The aggregated structures in Figure 2 are on the order of several microns wide and 100−300 nm in height, suggesting that they are essentially two-dimensional arrays of large particles with areas perhaps two particles deep. Previously reported SEM studies suggest that the naturally occurring macroscopic pigment consists of aggregates of such particles (*39*). Isolated large particles are observed surrounding the aggregate. A close inspection of the aggregated structure reveals significant substructure in the large particles in the form of entities with dimensions of ∼20−30 nm, comparable to the smaller particles discussed above. Such substructure is also supported by the manner in which the large particles are deformed from a spherical shape when they aggregate. Interestingly, it is more difficult to distinguish the composite small particles in CM AFM images, most like due to the greater force exerted by the imaging tip on the eumelanin during CM imaging than in TM imaging though possibly contributed to by the greater tip width and lower aspect ratio of the CM silicon nitride tip.

Figure 6 shows examples of an image that reveals a large deposit that appears to be partially or mostly amorphous. The lateral dimensions of the material in these structures are similar to those of the island aggregates displayed in Figure 2. However, none of the eumelanin structures we have described (i.e., filaments, small particles, large particles) are visible in the left image in Figure 6a except for what resembles a large particle nestled in the center of the structure. The right image shows a deposit in which amorphous materials appears to cover approximately half of an island aggregate of large particles. Such deposits are occasionally observed, and it is important to determine if such deposits are unique or if they share a structural morphology with the aggregated structures discussed above. If such deposits are structurally similar to the aggregates shown in Figure 2, then we would conjecture that in these cases, the eumelanin pigment is coated by remnants from cellular materials that were not removed during the isolation and purification process of the pigment. Analysis of the melanin extracts from *Sepia* ink, shows the presence of enzymes, salts and other leftover cellular material, including cellular membrane components (*46*). If this were indeed the case, then we would expect to find eumelanin aggregates if this top coating were removed. Figure 6b shows the effect of manipulating this material by the AFM tip. First the sample was cut along both the vertical (white arrows) and horizontal (black arrow) directions. The effect on the material was the same as that shown in Figure 3. Narrow regions were carved out, and the particle in the center of the image was disassembled. By scanning the surface at a rate faster than the tip can respond to height changes, one can displace a thin layer of material and probe the structure of the underlying surface. The second image in Figure 6 shows the result of such manipulation. Following 45 min of rapid scanning, the surface is similar to that of the island aggregates shown in Figure 2. Whether the coating material is oligomeric units of eumelanin that are not assembled into the substructure seen in the other aggregates or if this material is the remnant of other cellular components cannot be determined from these experiments.

At this point, it is interesting to conjecture about the mechanism by which the pigment assembles. The imaging data support the conclusion that there is a hierarchy in the

aggregation process. The large micron-sized island aggregates are comprised of structures that have a lateral dimension of ~150 nm. These particles are stable, yet the data show these species are aggregates themselves of individual smaller particles that are ~20 nm in dimension. Small particles of this size are also found isolated on the mica surface, further supporting a hierarchical aggregation. This is also consistent with recent SEM data (*39*). That eumelanin must be assembled from relatively small constituents is also supported by the images obtained of the MW fraction samples. Because anything ~3 nm or larger will not be passed through any of the ultrafiltration membranes, the fact that we see filaments and small particles after filtration must mean that these eumelanin structures must be reassembled from smaller molecules/constituents after filtering and perhaps during drying.

Starting at the molecular end, MALDI-TOF MS data argue that the molecular constituents of eumelanin are small, having masses on the order of ~1000 amu (*23*−*28*). Scattering data has suggested a fundamental aggregate of eumelanin composed of 3−4 π-stacked highly cross-linked, oligomers (Figure 7) (*29*). As outlined above, the existence of filaments and their dimensions argue in favor of such of model. However, a rigorous connection between the fundamental aggregates that the filament structure supports and the larger-scale particulate aggregates, i.e., the small and large particles, is not possible based on the imaging data alone. It is possible that the generation of the long filaments results from the evaporation of the eumelanin solution on the mica. There will be tradeoffs between forming large filaments and forming small aggregates of short, π-stacked structures. That such π-stacked structures can aggregate to form small particles is supported by the work of Gallas and co-workers, who describe TM AFM images of synthetic eumelanin deposited on glass treated with Mg^{2+} (*31*) in which aggregates ~1.5 nm in height, but 6−30 nm in width are observed. The large width of these structures may reflect a lateral association of fundamental aggregates and thereby provide a structural assembly that suggests that the small particles we observe here are made of localized π-stacked structures of fundamental aggregates. Ultimately, these small particles aggregate into ~150 nm spherical structures, from which the large pigment granules are assembled.

The above discussion provides a mechanism whereby a diversity in macroscopic structure can be obtained from a fairly uniform molecular building block. However, it is unlikely that melanin is derived from a unique well-defined oligomeric structure. The collective data, however, argue that the major building block of eumelanin pigments is a small planar oligomer containing 4−8 monomer units. Due to the chemical diversity of the DHI and DHICA molecular building blocks, the oligomer can have a range of different chemical functionality, with quinone, semiquinone, and hydroquinone substitutents likely being the mostly photoreactive (*47*−*52*). The assembly of such structures into the macroscopic pigment can then result in significant chemical heterogeneity and, as a result, enable the pigment to perform a diverse range of functions.

In conclusion, the macroscopic morphology of *Sepia* eumelanin is determined by the aggregation behavior of its most basic component, the oligomeric molecular building block composed of the precursors DHI and DHICA. The observation of filaments upon the drying of stock and low mass weight fractions support the conclusion that this oligomeric molecular unit is highly cross-linked with maximum dimensions of 4 × 10 Å and that it preferentially aggregates into fundamental aggregates of 3−4 π-stacked oligomers. A detailed study of images of the pigment reveals the presence individual particles and aggregates. Manipulation of the materials using the AFM tip shows that the larger particles (~150 nm lateral dimension) are not fundamental eumelanin units but are instead aggregates of molecules that are small compared to the AFM tip dimensions. This is also consistent with the existence of the filaments and argues that the different morphologies observed are built from a common set of molecules. Further work is needed to identify the chemical structure of molecular building blocks and thereby develop an understanding of the forces that govern the formation of the observed structures.

ACKNOWLEDGMENT

We thank Drs. Susan Forest and J. Brian Nofsinger for their insights into the photochemical reactions of mass-selected eumelanin fractions.

REFERENCES

1. Zeise, L., Chedekel, M. R., and Fitzpatrick, T. B. (1995) *Melanin: its role in human protection*, Valdnmar, Overland Park.
2. Prota, G. (1992) *Melanins and Melanogenesis*, Academic Press, San Diego.
3. Simon, J. D. (2000) *Acc. Chem. Res. 33*, 307−313.
4. Hill, H. Z. (1992) *BioEssays 14*, 49−56.
5. Sarna, T. (1992) *Photochem. Photobiol. B 12*, 215−258.
6. Hill, H. Z., and Hill, G. J. (1987) *Pigment Cell Res. 1*, 163−170.
7. Hubbard-Smith, K., Hill, H. Z., and Hill, G. J. (1992) *Radiat. Res. 130*, 160−165.
8. Menon, I. A., and Haberman, H. F. (1977) *Br. J. Dermatol. 97*, 109−112.
9. Hunt, G., Kyne, S., Ito, S., Wakamatsu, K., Todd, C., and Thody, A. J. (1995) *Pigment Cell Res. 8*, 202−208.
10. Sealy, R. C., Felix, C. C., Hyde, J. S., and Swartz, J. M. (1980) in *In Free Radicals in Biology* (Pryor, W. A., Ed.) pp 205−259, Academic Press, New York.
11. Thody, A. J., Higgins, E. M., Wakamatsu, K., Ito, S., Burchill, S. A., and Marks, J. M. (1991) *J. Invest. Dermatol. 97*, 340−344.
12. Ito, S. (1993) *J. Invest. Dermatol. 100*, 116S-171S.
13. Ito, S., and Wakamatsu, K. (1998) *Pigment Cell Res. 11*, 120−126.
14. Ito, S. (1986) *Biochim. Biophys. Acta 883*, 155−161.
15. Tsukamoto, K., Palumbo, A., M., d. I., Hearing, V. J., and Prota, G. (1992) *Biochem. J. 286*, 491−495.
16. Ozeki, H., Wakamatsu, K., Ito, S., and Ishiguro, I. (1997) *Anal. Biochem. 248*, 149−157.
17. Borges, C. R., Roberts, J. C., Wilkins, D. G., and Rollins, D. E. (2001) *Anal. Biochem. 290*, 116−125.
18. Ito, S., and Jimbow, K. (1983) *J. Invest. Dermatol. 80*, 268−272.
19. Ito, S., and Fujita, K. (1985) *Anal. Biochem. 144*, 527−536.
20. Prota, G., Lamoreux, M. L., Muller, J., Kobayashi, T., Napolitano, A., Vincensi, M. R., Sakai, C., and Hearing, V. J. (1995) *Pigment Cell Res. 8*, 153−163.
21. Prota, G., Hu, D.-N., Vincensi, M. R., McCormick, S. A., and Napolitano, A. (1998) *Exp. Eye Res. 67*, 293−299.
22. Kollias, N., Sayre, R. M., Zeise, L., and Chedekel, M. R. (1991) *J. Photochem. Photobiol. B 9*, 135−160.
23. Bertazzo, A., Costa, C., and Allegri, G. (1995) *Eur. Mass Spectrom. 1*, 305−311.

24. Bertazzo, A., Costa, C. V. L., Allegri, G., Schiavolin, M., Favretto, D., and Traldi, P. (1999) *Rapid Commun. Mass Spectrom. 13*, 542−547.
25. Costa, C., Bertazzo, A., Allegri, G., Toffano, G., Curcuruto, O., and Traldi, P. (1992) *Pigment Cell Res. 5*, 122−131.
26. Kroesche, C., and Peter, M. G. (1996) *Tetrahedron 52*, 3947−3952.
27. Napolitano, A., Pezzella, A., Prota, G., Seraglia, R., and Traldi, P. (1996) *Rapid Commun. Mass Spectrom. 10*, 468−472.
28. Pezzella, A., Napolitano, A., d'Ischia, M., Prota, G., Seraglia, R., and Traldi, P. (1997) *Rapid Commun. Mass Spectrom. 11*, 368−372.
29. Cheng, J., Moss, S. C., and Eisner, M. (1994) *Pigment Cell Res. 7*, 263−273.
30. Cheng, J., Moss, S. C., Eisner, M., and Zschack, P. (1994) *Pigment Cell Res. 7*, 255−262.
31. Gallas, J. M., Zajac, G. W., Sarna, T., and Stotter, P. L. (2000) *Pigment Cell Res. 13*, 99−108.
32. Zajac, G. W., Gallas, J. M., Cheng, J., Eisner, M., Moss, S. C., and Alvarado-Swaisgood, A. E. (1994) *Biochim. Biophys. Acta 1199*, 271−278.
33. Zajac, G. W., Gallas, J. M., and Alvarado-Swaisgood, A. E. (1994) *J. Vacuum Sci. Technol. B 12*, 1512−1516.
34. Gallas, J. M., Littrell, K. C., Seifert, S., Zajac, G. W., and Thiyagarajan, P. (1999) *Biophys. J. 77*, 1135−1142.
35. Palumba, A., Di Cosmo, A., Gesualdo, I., and Hearing, V. J. (1997) *Biochem. J. 323*, 749−756.
36. Zeise, L., Murr, B. L., and Chedekel, M. R. (1992) *Pigment Cell Res. 5*, 132−142.
37. Clancy, C. M. R., Hanks, R. K., and Simon, J. D. (2000) *J. Phys. Chem. B 104*, 7871−7873.
38. Boussaad, S., Tao, N. J., and Arechabaleta, R. (1997) *Chem. Phys. Lett. 280*, 397−403.
39. Nofsinger, J. B., Forest, S. E., Eibest, L., Gold, K. A., and Simon, J. D. (2000) *Pigment Cell Res. 13*, 180−185.
40. Vitkin, I. A., Woolsey, J., Wilson, B. C., and Anderson, R. R. (1994) *Photochem. Photobiol 59*, 455−462.
41. Ariga, K., Kikuchi, J., Naito, M., Koyama, E., and Yamada, N. *Langmuir 16*, 4929−4939.
42. Kayed, R., Bernhagen, J., Greenfield, N., Sweimeh, K., Brunner, H., Voelter, W., and Kapurniotu, A. (1999) *J. Mol. Biol. 287*, 781−796.
43. Rinia, H. A., Kik, R. A., Demel, R. A., Snel, M. M. E., Killian, J. A., van der Eerden, J. P. J. M., and de Kruijff, B. (2000) *Biochemistry 39*, 5852−5858.
44. Shibata-Seki, T., Masai, J., Ogawa, Y., Sato, K., and Yanagawa, H. (1998) *Appl. Phys. A 66*, S625−S629.
45. Van Mau, M., Vie, V. C., L., Leseniewska, E., Heitz, F., and LeGrimellec, C. (1999) *Membr. Biol. 167*, 241−249.
46. Zeise, L., Addison, R. B., and Chedekel, M. R. (1992) *Pigment Cell Res. 2*, 48−53.
47. Korytowski, W., Kalyanaraman, B., Menon, I. A., Sarna, T., and Sealy, R. C. (1986) *Biochim. Biophys. Acta 882*, 145−153.
48. Korytowski, W., Pilas, B., Sarna, T., and Kalyanaraman, B. (1987) *Photochem. Photobiol. 45*, 185−190.
49. Sarna, T., Menon, I. A., and Sealy, R. C. (1984) *Photochem. Photobiol. 39*, 805−809.
50. Sarna, T., and Sealy, R. C. (1984) *Arch. Biochem. Biophys. 232*, 574−578.
51. Sarna, T., Pilas, B., Land, E. J., and Truscott, T. G. (1986) *Biochim. Biophys. Acta 883*, 162−170.
52. Sealy, R. C., Sarna, T., Wanner, E. J., and Reszka, K. (1984) *Photochem. Photobiol. 40*, 453−459.

BI010786T